

## Computation of internal optical forces using the Helmholtz tensor

Liyong Cui<sup>①,1</sup>, Neng Wang<sup>2,\*</sup>, and Jack Ng<sup>3,†</sup>

<sup>1</sup>Hunan Provincial Laboratory of Flexible Electronic Materials Genome Engineering, Changsha University of Science and Technology, Changsha 410014, China

<sup>2</sup>Institute of Microscale Optoelectronics, Shenzhen University, Shenzhen 518060, China

<sup>3</sup>Department of Physics, Southern University of Science and Technology, Shenzhen 518055, China



(Received 4 February 2020; revised 4 June 2021; accepted 11 June 2021; published 8 July 2021)

The computation of the internal optical force density inside a metamaterial is a controversial subject. Various stress tensors have been proposed; however, each yields a different result. Here, by adopting the Helmholtz stress tensor and effective medium theories, we calculated the force densities acting on metamaterials composed of a one-dimensional deep-subwavelength dielectric-air multilayer or a two-dimensional square lattice cylinder array. Our results agree remarkably with the benchmarking noneffective medium treatment. The key is to treat the effective parameters as operators; i.e., take different values for the wave with different  $k$  vector. This work provides an approach to compute the internal optical force in metamaterials.

DOI: [10.1103/PhysRevA.104.013508](https://doi.org/10.1103/PhysRevA.104.013508)

### I. INTRODUCTION

At the microscopic level, the bidirectional interaction of light and matter is governed by the microscopic Maxwell equations, which describe how matter influences the flow of light, and the Lorentz force law (equivalent to Maxwell stress tensor, MST), which describes how light influences the path of matter. However, such approach is impractical for nano- or bigger structures. The macroscopic number of nuclei and electrons makes the computation impossible. Here, the macroscopic Maxwell equations can be applied instead of the microscopic Maxwell equations, which correctly describe the flow of light in the presence of materials. The light-induced forces acting on an object in vacuum or air can also be computed by a surface integral of the Maxwell stress tensor, with the required microscopic field being approximated by the macroscopic field, because they are approximately equal in vacuum or air.

The problem arises when one considers the internal optical force densities distributed over the volume of a piece of metamaterial. For simplicity, we shall focus on two examples: first, a one-dimensional metamaterial comprising a periodic collection of dielectric slabs in air, as shown in Fig. 1(a); second, a two-dimensional metamaterial consisting of a square lattice of dielectric cylinders embedded in air; see Fig. 8. Throughout the paper, for the one-dimensional metamaterial, the number of slabs, the thickness of the slabs, the lattice constant, and the wavelength of light are 50, 5, 10, and 700 nm, respectively. The lattice constant of the two-dimensional square array of the cylinder is 10 nm, the radii of the cylinders are 3 nm, and the incident wavelength is 600 nm. Such deep-subwavelength spacings ensured the accuracy of the effective medium

theories, so any error in the calculation should be attributed to the stress tensor rather than the effective medium theories.

In principle, to evaluate the total optical force, one could use the time-averaged “macroscopic” MST [1]:

$$T_{ik.M} = \frac{1}{2} \text{Re} \left[ \varepsilon_0 E_{M,i} E_{M,k}^* + \frac{B_{M,i} B_{M,k}^*}{\mu_0} - \frac{1}{2} \left( \varepsilon_0 |\mathbf{E}_M|^2 + \frac{|\mathbf{B}_M|^2}{\mu_0} \right) \delta_{ik} \right], \quad (1)$$

which has the same form as the true MST, except that  $\mathbf{E}_M$  and  $\mathbf{B}_M$  are the macroscopic fields rather than the microscopic fields. We stress that in vacuum or air, the difference between the microscopic field and the macroscopic field is small, so Eq. (1) is valid. However, such approach can be computationally very heavy for large structures. Worse, if the objects are physically connected such that it is impossible for the integration surface to enclose a single object without overlapping with the materials, then the macroscopic MST approach in Eq. (1) will be inapplicable, because inside a material, the macroscopic and microscopic electromagnetic fields can be very different. To cope with such issues, a stress tensor that works inside the metamaterials is required. In order to reduce the amount of computation required, we shall treat the metamaterial as a homogeneous effective medium without directly considering the microstructures. Then we solve for the effective medium fields (which can be regarded as the spatially averaged macroscopic fields) through applying the standard electromagnetic boundary conditions. Then, we apply the Helmholtz stress tensor (HST) evaluated by the effective medium fields to compute the internal optical force densities. Such an approach is much more efficient as one just needs to handle a single homogeneous scatterer, rather than solving the scattering problem of the structured metamaterials.

\*nwang17@szu.edu.cn

†wuzh3@sustech.edu.cn

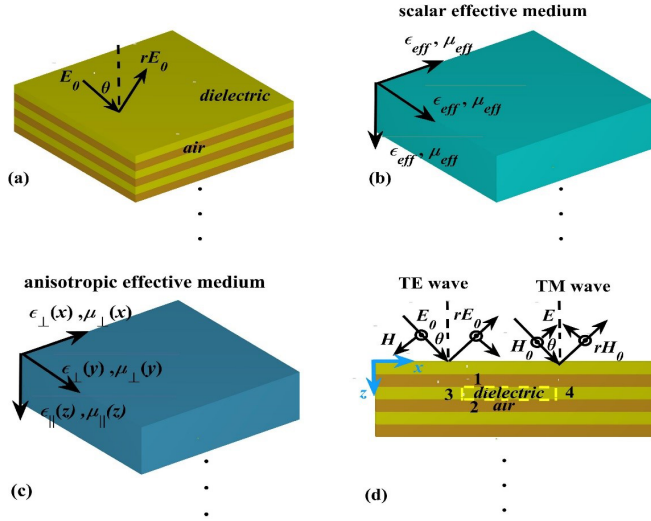


FIG. 1. (a) Schematic illustration for a linearly polarized plane wave with a modest intensity of  $1.33 \times 10^{-2} \text{ mW/m}^2$  incident on the dielectric-air multilayer. (b) In the long-wavelength limit, the multilayer structure shown in (a) can be regarded as a scalar homogeneous effective medium. (c) The multilayer structure can also be considered as an anisotropic effective medium characterized by tensor permittivity and permeability. (d) Front view of (a) with TE and TM incident plane waves.

We are aware that several stress tensors [2–8] were proposed to calculate the optical force densities, which include, but are not limited to, Minkowski, Einstein-Laub, and Helmholtz stress tensors. While most of them give the same total optical force, when calculating the internal optical force densities inside the scatterer, or the total force acting on a scatterer located inside a complex fluid, different tensors yield different results [9–18]. Here, we show that the HST, when its electrostriction and magnetostriction terms are treated as operators, gives results that agree remarkably with the benchmarking macroscopic MST, thereby verifying its correctness. We stress that our effective medium theory calculation of internal optical force densities is much more computationally efficient compared to that using the macroscopic MST, since the latter requires one to solve for the macroscopic fields of the structured materials, while the former only requires one to calculate the effective medium fields from a homogeneous object. The accurate computation of the internal optical force densities enables us to consider the optomechanical effect in metamaterials [19–21].

## II. HOMOGENIZATION OF THE MULTILAYER STRUCTURE

The multilayer structure can be effectively represented by a scalar effective medium approach (see Sec. II A below) or an anisotropic effective medium approach (see Sec. II B below). We shall see that the HST gives correct results under both types of effective medium descriptions.

### A. Scalar effective medium approach

Effective medium theory is widely employed in describing the optical properties of materials composed of a collection of

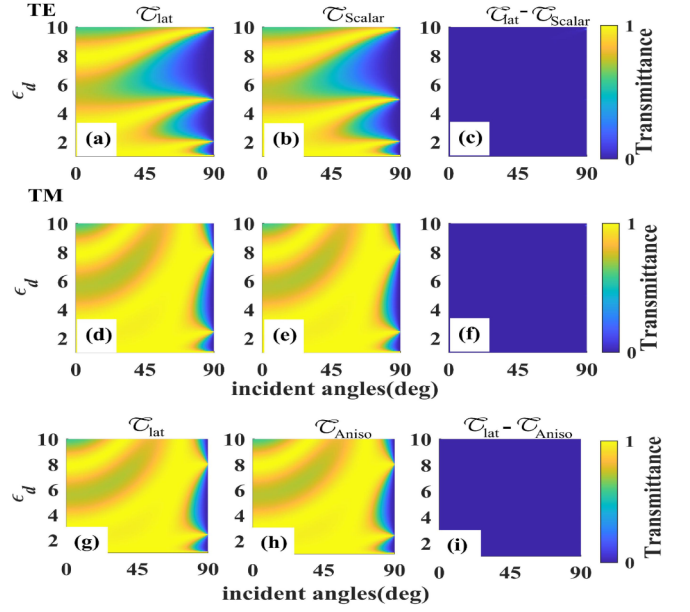


FIG. 2. (a) Transmittance ( $\mathcal{T}$ ) for the lattice structure shown in Fig. 1(a) when illuminated by a TE plane wave. (b) Transmittance for the scalar effective medium shown in Fig. 1(b) illuminated by a TE plane wave. (c) The difference between the transmittances shown in (a) and (b). (d) Transmittance for the lattice structure shown in Fig. 1(a) illuminated by a TM plane wave. (e) Transmittance for the scalar effective medium shown in Fig. 1(b) illuminated by a TM plane wave. (f) The difference between the transmittance shown in (d) and (e). (g) Transmittance for the real lattice structure shown in Fig. 1(a) when illuminated by a TM plane wave. (h) Transmittance for the anisotropic effective medium shown in Fig. 1(c) illuminated by a TM plane wave. (i) The difference between the transmittance shown in (g) and (h). The result indicates that these effective medium theories are accurate in computing the transmittance.

subwavelength elements. As an example, a structure consisting of alternating dielectric-air slabs is depicted in Fig. 1(a). The relative permeabilities of the dielectric and air are taken to be  $\mu_d = \mu_a = 1$ , where the subscripts  $d$  and  $a$  stand for dielectric and air, respectively. The structure can be treated as a homogeneous material in the long-wavelength limit, as shown in Fig. 1(b). Treating the effective relative permittivity and permeability as scalars [22], for TE polarization they are

$$\epsilon_{\text{eff}} = \rho\epsilon_d + (1 - \rho)\epsilon_a, \quad \mu_{\text{eff}} = 1, \quad (2)$$

while for TM polarization they are

$$\epsilon_{\text{eff}} = \rho\epsilon_d + (1 - \rho)\epsilon_a, \\ \mu_{\text{eff}} = 1 - \frac{\rho(\rho - 1)(\epsilon_a - \epsilon_d)^2}{\epsilon_a\epsilon_d[\epsilon_a(\rho - 1) - \rho\epsilon_d]} \sin^2\theta, \quad (3)$$

where  $\theta$  is the incident angle measured with respect to the slab's normal,  $\epsilon_d$  ( $\epsilon_a$ ) is the relative permittivity of the dielectric (air),  $\rho = d_d/(d_d + d_a)$  is the filling fraction of the dielectrics with  $d_d$  ( $d_a$ ) being the thickness of dielectric (air).

Figure 2 demonstrates the validity of the scalar effective medium approach in calculating the transmittance. The transmittance of the multilayer structures [as shown in Fig. 1(a)] for TE and TM polarized incident waves is

plotted in Figs. 2(a) and 2(d), respectively. For comparison, the transmittance for the corresponding effective media [as shown in Fig. 1(b)] for TE and TM polarized waves is plotted in Figs. 2(b) and 2(e), respectively. The incident angle ranges from  $0^\circ$  to  $89^\circ$ , and the relative permittivity of the dielectric ranges from 1 to 10. The differences between the two approaches are given in Figs. 2(c) and 2(f), which are vanishing small ( $\sim 10^{-8}$ – $10^{-4}$ ), illustrating the accuracy of the scalar effective medium model.

### B. Anisotropic effective medium approach

The multilayer dielectric-air metamaterial shown in Fig. 1(a) can also be considered as an anisotropic medium using the Maxwell-Garnett effective medium theory. The relative permittivity and permeability possess tensor forms [23–27]:

$$\varepsilon = \begin{pmatrix} \varepsilon_{\perp} & 0 & 0 \\ 0 & \varepsilon_{\perp} & 0 \\ 0 & 0 & \varepsilon_{\parallel} \end{pmatrix},$$

$$\mu = \begin{pmatrix} \mu_{\perp} & 0 & 0 \\ 0 & \mu_{\perp} & 0 \\ 0 & 0 & \mu_{\parallel} \end{pmatrix} = \begin{pmatrix} 1 & 0 & 0 \\ 0 & 1 & 0 \\ 0 & 0 & 1 \end{pmatrix}, \quad (4)$$

where

$$\varepsilon_{\perp} = \varepsilon_{\text{eff}x} = \varepsilon_{\text{eff}y} = \frac{(d_d \varepsilon_d + d_a \varepsilon_a)}{d_d + d_a},$$

$$\varepsilon_{\parallel} = \varepsilon_{\text{eff}z} = \frac{\varepsilon_a \varepsilon_d (d_a + d_d)}{(\varepsilon_a d_d + \varepsilon_d d_a)}, \quad (5)$$

are the permittivity components perpendicular and parallel to the array axis, respectively [23]. Again, we confirm the validity of Eq. (5) by considering the transmittance. Figure 2(g) plots the transmittance for the real structures. Those for the effective medium with constitutive parameters given by Eq. (5) are plotted in Fig. 2(h). A broad range of incident angles (ranging from  $0^\circ$  to  $89^\circ$ ) is considered, and the relative permittivity of the dielectric ranges from 1 to 10. The differences between the two approaches are plotted in Fig. 2(i), which are vanishing small ( $\sim 10^{-8}$ – $10^{-4}$ ), illustrating the accuracy of the anisotropic effective medium model.

## III. DERIVATION OF ELECTROSTRICTION AND MAGNETOSTRICTION

### A. Helmholtz stress tensors

HST [7] can be derived based on the principle of virtual work. Its expression specifically for amorphous and crystalline media can be found in Refs. [28–39]. By treating the effective parameters as operators, here we extended the form of the HST as (see Appendixes A and B for details)

$$T_{ik,H} = \frac{1}{2} \text{Re} \left\{ E_i D_k^* - \frac{1}{2} (\mathbf{E} \cdot \mathbf{D}^*) \delta_{ik} - \frac{1}{2} \mathbf{E} \cdot \sum_n \frac{\partial \varepsilon_{\text{eff},n}}{\partial u_{ik}} \mathbf{E}_n + H_i B_k^* - \frac{1}{2} (\mathbf{H} \cdot \mathbf{B}^*) \delta_{ik} - \frac{1}{2} \mathbf{H} \cdot \sum_n \frac{\partial \mu_{\text{eff},n}}{\partial u_{ik}} \mathbf{H}_n \right\}, \quad (6)$$

where  $\varepsilon_{\text{eff},n}$ ,  $\mu_{\text{eff},n}$  are the relative permittivity and permeability (can be scalar or tensor) of the effective medium for the  $n$ th plane wave component and  $u_{ik}$  represents the strain tensor defined as  $u_{ik} = \frac{1}{2} (\partial u_i / \partial x_k + \partial u_k / \partial x_i)$ , with  $\vec{u}(\vec{x})$  being a displacement vector [35];  $\partial \varepsilon_{\text{eff}} / \partial u_{ik}$  and  $\partial \mu_{\text{eff}} / \partial u_{ik}$  [30–38] are the electrostriction and magnetostriction, which describe the change in the permittivity and permeability due to the deformation of the effective dielectric solid. Here,  $\mathbf{E}$  and  $\mathbf{H}$  denote the effective electromagnetic fields, which are equal to the spatial average of the macroscopic fields. We remark that the electromagnetic fields in MST are macroscopic fields throughout this paper.

### B. Derivation of electrostriction and magnetostriction

For the layered metamaterial, the deformation by stretching can be described by

$$u = \frac{z(\Lambda - \Lambda_0)}{\Lambda_0}, \quad (7)$$

where  $\Lambda_0$  and  $\Lambda$  are the lattice constants before and after deformation, respectively. The strain tensor is given by

$$u_{zz} = \frac{\partial u}{\partial z} = \frac{(\Lambda - \Lambda_0)}{\Lambda_0}. \quad (8)$$

For the scalar effective medium approach, according to Eqs. (2) and (3), the electrostriction for both TE and TM polarizations is given by

$$\frac{\partial \varepsilon_{\text{eff}}}{\partial u_{zz}} = \frac{\partial \varepsilon_{\text{eff}}}{\partial \Lambda} \frac{\partial \Lambda}{\partial u_{zz}} \approx \frac{d_d (\varepsilon_a - \varepsilon_d)}{\Lambda_0} = \rho (\varepsilon_a - \varepsilon_d). \quad (9)$$

The magnetostriction term for TE polarization vanishes because  $\mu_{\text{eff}} \equiv 1$ . However, the magnetostriction term for TM polarization is nonzero and is given by

$$\begin{aligned} \frac{\partial \mu_{\text{eff}}}{\partial u_{zz}} &= \frac{\partial \mu_{\text{eff}}}{\partial \Lambda} \frac{\partial \Lambda}{\partial u_{zz}} = \frac{d_d (\varepsilon_a - \varepsilon_d)^2 (d_a^2 \varepsilon_a - d_d^2 \varepsilon_d) \sin^2 \theta}{\varepsilon_a \varepsilon_d (d_a \varepsilon_a + d_d \varepsilon_d)^2 (d_a + d_d)}, \\ &= \frac{(\varepsilon_a - \varepsilon_d)^2 \rho [\varepsilon_a (\rho - 1)^2 - \varepsilon_d \rho^2]}{\varepsilon_a \varepsilon_d [\varepsilon_a (1 - \rho) + \varepsilon_d \rho]^2} \sin^2 \theta. \end{aligned} \quad (10)$$

Therefore, the magnetostriction term depends on the incident angle  $\theta$  for TM polarization, in contrast to both electrostriction and magnetostriction terms being independent of the incident angle for TE polarization.

For the anisotropic effective medium approach, combining Eqs. (4), (5), (7), and (8), the electrostriction is obtained as

$$\begin{aligned} \frac{\partial \varepsilon_{\text{eff}x}}{\partial u_{zz}} &= \frac{\partial \varepsilon_{\text{eff}y}}{\partial u_{zz}} = \frac{d_d (\varepsilon_a - \varepsilon_d)}{d_d + d_a}, \\ \frac{\partial \varepsilon_{\text{eff}z}}{\partial u_{zz}} &= \frac{d_a (d_a + d_d) \varepsilon_a \varepsilon_d (\varepsilon_a - \varepsilon_d)}{(d_d \varepsilon_a + d_a \varepsilon_d)^2}, \end{aligned} \quad (11)$$

and the magnetostriction vanishes since the effective permeability is always 1.

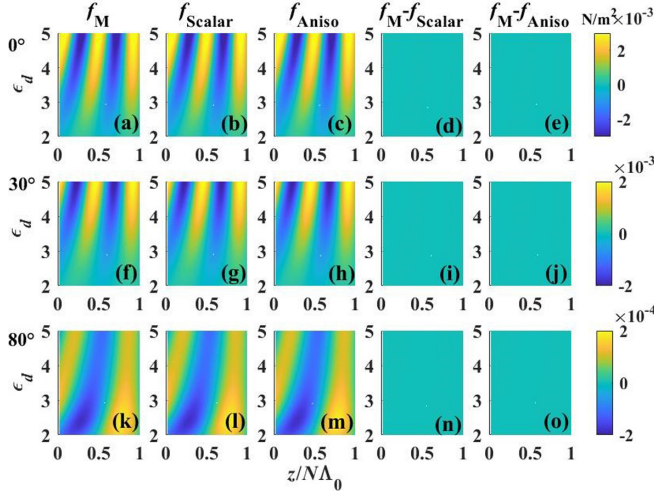


FIG. 3. The optical force densities acting on each slab versus permittivity of the slabs. The incident light is TM polarized. The first, second, and third columns denote  $f_M$ ,  $f_{\text{Scalar}}$ , and  $f_{\text{Aniso}}$ , respectively. The fourth and fifth columns denote the difference between  $f_M$  and  $f_{\text{Scalar}}$ , and  $f_M$  and  $f_{\text{Aniso}}$ , respectively. The first, second, and third rows denote the results when the incident angles are  $0^\circ$ ,  $30^\circ$ , and  $80^\circ$ , respectively. The result indicates that our HST approach is accurate irrespective of the type of effective medium employed.  $\Lambda_0$  denotes the lattice constant.

#### IV. INTERNAL OPTICAL FORCE CALCULATION OF MULTILAYERED STRUCTURE

##### A. Single incident beam

The time-averaged optical force can be calculated using MST over a surface integral:

$$\mathbf{F} = \oint_S \vec{\mathbf{T}} \cdot d\mathbf{S}. \quad (12)$$

For the parallel, infinitely large slabs in air, it can be simplified to

$$\mathbf{F} = \sum_{i=1}^6 \int_{\text{surface } i} \vec{\mathbf{T}} \cdot d\mathbf{a} = \int_{\text{surface } 1} \vec{\mathbf{T}} \cdot d\mathbf{a} + \int_{\text{surface } 2} \vec{\mathbf{T}} \cdot d\mathbf{a}, \quad (13)$$

where the surfaces 1–4 are depicted in Fig. 1(d) by the yellow dotted lines and the surfaces 5 and 6 are the front and back covers of the rectangle formed by surfaces 1–4. According to the Bloch theorem, the contributions from surfaces 3 and 4, and 5 and 6 (which are not shown) will cancel each other.

For a single TM polarized incident wave, the force densities calculated by HST using the scalar effective medium approach are compared with the benchmarks calculated by MST, as shown in Fig. 3. The relative permittivity of the slabs  $\epsilon_d$  ranges from 2 to 5, and the filling ratio is 0.5. The force densities calculated by HST with the scalar and anisotropic effective medium approaches are denoted by  $f_{\text{Scalar}}$  and  $f_{\text{Aniso}}$ , respectively. The benchmarks calculated by MST are denoted by  $f_M$ . The incident angles in Fig. 3 are  $0^\circ$  (first row),  $30^\circ$  (second row), and  $80^\circ$  (third row).  $f_M - f_{\text{Scalar}}$  and  $f_M - f_{\text{Aniso}}$  are plotted in the fourth and fifth columns. We can see all results calculated by HST agree excellently with the benchmarking  $f_M$ .

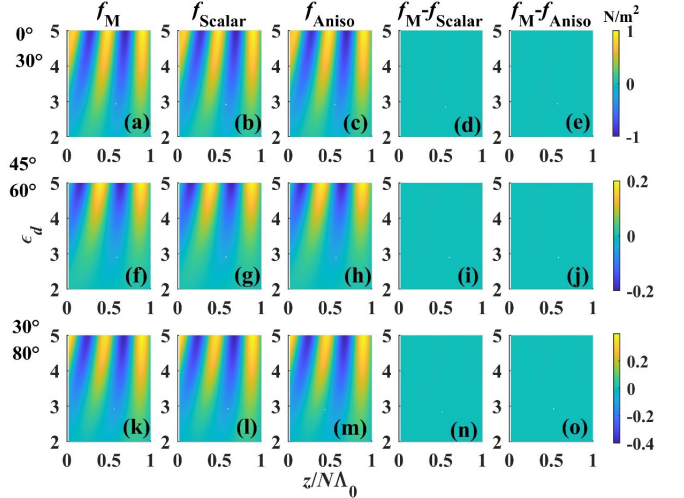


FIG. 4. The force densities when illuminated by two TM incident beams at different incident angles. The first, second, and third columns denote  $f_M$ ,  $f_{\text{Scalar}}$ , and  $f_{\text{Aniso}}$ , respectively. The fourth and fifth columns denote the difference between  $f_M$  and  $f_{\text{Scalar}}$ , and  $f_M$  and  $f_{\text{Aniso}}$ , respectively. The incident angles of the two beams for the first, second, and third rows are  $0^\circ$  and  $30^\circ$ ,  $45^\circ$  and  $60^\circ$ , and  $30^\circ$  and  $80^\circ$ , respectively. Other parameters are the same as Fig. 3.

##### B. Two incident beams

To compute the internal optical force densities accurately, it is necessary to treat the electrostriction and magnetostriction as operators: The total field is decomposed into a series of plane waves, and each plane wave component is associated to a different value of electrostriction and magnetostriction, as in Eq. (6).

For the anisotropic effective medium approach, since the magnetostriction term vanishes, Eq. (6) can be further simplified to

$$\begin{aligned} T_{zz,H} = & \frac{1}{2} \text{Re} \left[ \epsilon_0 \sum_n E_{z,n} \sum_n \epsilon_{\text{eff},z,n} E_{z,n}^* \right. \\ & - \frac{1}{2} \epsilon_0 \sum_n E_{x,n} \sum_n \left( \epsilon_{\text{eff},x,n} + \frac{\partial \epsilon_{\text{eff},x,n}}{\partial u_{zz}} \right) E_{x,n}^* \\ & - \frac{1}{2} \epsilon_0 \sum_n E_{z,n} \sum_n \left( \epsilon_{\text{eff},z,n} + \frac{\partial \epsilon_{\text{eff},z,n}}{\partial u_{zz}} \right) E_{z,n}^* \\ & \left. - \frac{1}{2} \mu_0 \left| \sum_n H_{y,n} \right|^2 \right]. \quad (14) \end{aligned}$$

For illustrative purposes, we consider two incident plane waves. Force densities exerted by two incident waves at different incident angles are computed and plotted in Fig. 4. The parameters are the same as those in Fig. 3. The first, second, and third columns denote  $f_M$ ,  $f_{\text{Scalar}}$ , and  $f_{\text{Aniso}}$ , respectively. The fourth and fifth columns are the difference between  $f_M$  and  $f_{\text{Scalar}}$ , and  $f_M$  and  $f_{\text{Aniso}}$ . The incident angles of the two plane waves for the first, second, and third rows are, respectively,  $0^\circ$  and  $30^\circ$ ,  $45^\circ$  and  $60^\circ$ , and  $30^\circ$  and  $80^\circ$ . Clearly,  $f_{\text{Scalar}}$  and  $f_{\text{Aniso}}$  are matching very well with the benchmarks  $f_M$ , indicating that even when the multilayer structure is illumi-

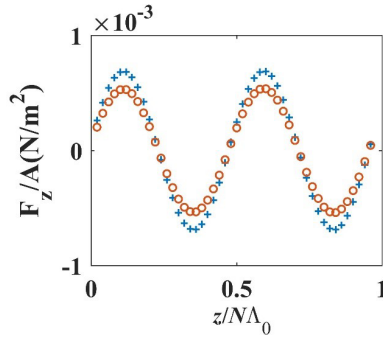


FIG. 5. Optical force densities calculated by the approach in Ref. [30] (red circles) and our approach (blue plus signs) with two incident beams at  $30^\circ$  and  $60^\circ$ ,  $\epsilon_d = 4$ .

nated by multiple incident beams, the internal optical force densities can still be computed accurately, if the electrostriction and magnetostriction are treated as operators, which takes all the wave vectors with appropriate weighing into consideration. We also compute the optical force densities using the approach of Ref. [30] where an effective  $k$  is introduced to determine the electrostriction and magnetostriction. The results are compared with our results, as shown in Fig. 5. Clearly, the results by the approach of Ref. [30] deviate remarkably from the benchmarking  $f_M$ .

For TE polarization, both the electrostriction and magnetostriction are  $k$  independent. Figures 6 and 7 show the force densities when illuminated by single or double incident TE plane waves, with all the parameters the same as Figs. 3 and 4. Clearly, the force densities calculated by HST agree remarkably with the benchmarking results computed by MST.

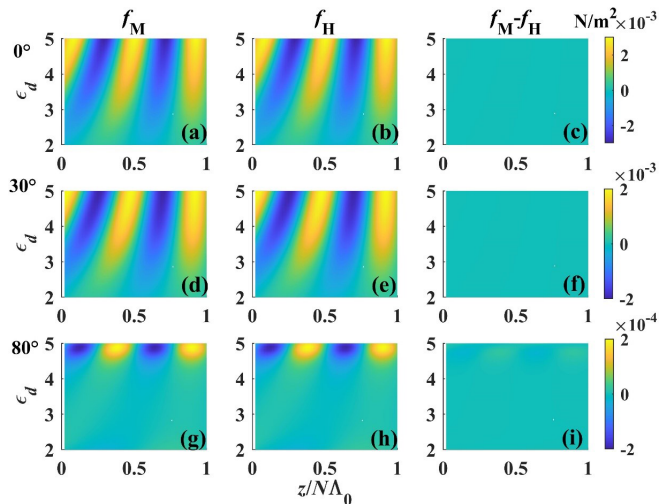


FIG. 6. For the one-dimensional (1D) multilayer structure, the optical force densities acting on each slab versus the permittivity of the slabs. The incident light is TE polarized. The left and middle columns are  $f_M$  and  $f_H$ , respectively. The third column denotes the difference between  $f_M$  and  $f_H$ . The first, second, and third rows denote the results when the incident angles are  $0^\circ$ ,  $30^\circ$ , and  $80^\circ$ . The result indicates that our HST approach is accurate.

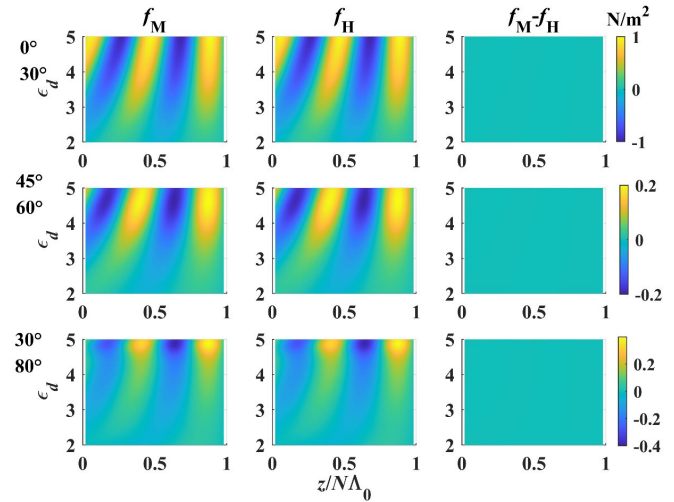


FIG. 7. For the 1D multilayer structure, the force densities with two TE polarized incident beams at different incident angles. The left and middle columns denote  $f_M$  and  $f_H$ , respectively. The third column denotes the difference between  $f_M$  and  $f_H$ . The incident angles of the two beams for the first, second, and third rows are  $0^\circ$  and  $30^\circ$ ,  $45^\circ$  and  $60^\circ$ , and  $30^\circ$  and  $80^\circ$ , respectively. All the parameters are the same as Fig. 4.

## V. INTERNAL OPTICAL FORCE DENSITIES CALCULATION FOR PERIODIC CYLINDER ARRAY

We also considered an effective slab made from a two-dimensional (2D) photonic crystal with dielectric cylinders arranged into a square lattice embedded in air; see Fig. 8. The 2D photonic crystal is periodic along the  $x$  direction, possesses 30 periods along the  $z$  direction, and the cylinders are infinitely long. The lattice constant is  $\Lambda_0 = 10$  nm and the incident wavelength is 600 nm. The relative permittivity, permeability, and radius of the cylinders are  $\epsilon_c = 8$ ,  $\mu_c = 1$ , and  $r_c = 0.3\Lambda_0$ , respectively. According to the Clausius-Mossotti relation, the effective permittivity for TM polarization takes the form  $\epsilon_{\text{eff}x} = \epsilon_{\text{eff}z} = \epsilon_{\text{eff}} =$

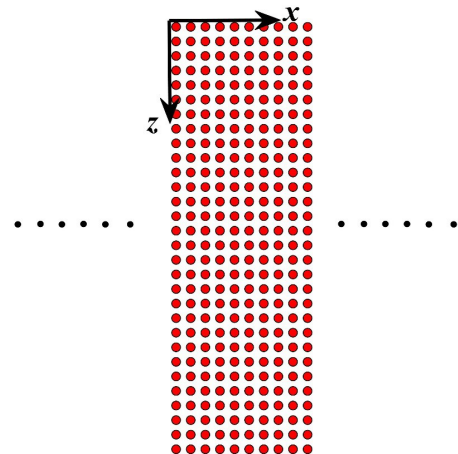


FIG. 8. Schematic of a 2D photonic crystal embedded in air. The cylinder is infinitely long along the  $y$  direction. The photonic crystal is periodic along the  $x$  direction and has 30 periods along the  $z$  direction. The red area denotes the cylinder with permittivity  $\epsilon_c = 8$ .

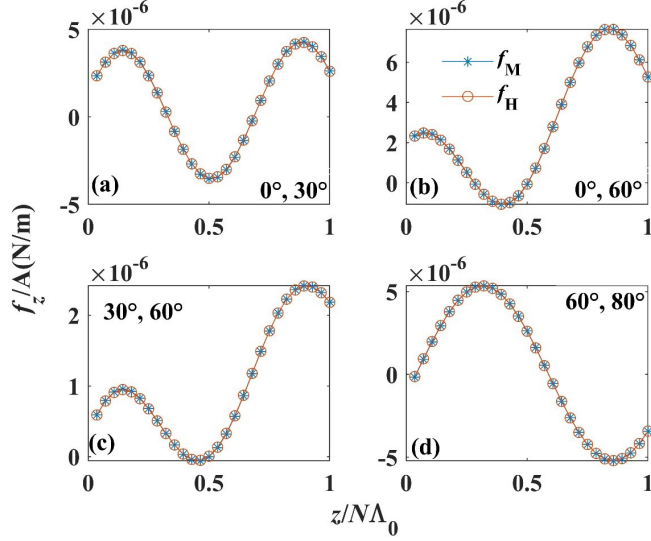


FIG. 9. Force densities acting on a slab consisting of 2D cylinder array (see Fig. 8) and its effective medium. For two TM incident waves with incident angles (a)  $0^\circ$  and  $30^\circ$ , (b)  $0^\circ$  and  $60^\circ$ , (c)  $30^\circ$  and  $60^\circ$ , and (d)  $60^\circ$  and  $80^\circ$ , respectively. Remarkable agreements are achieved.

$(1 + pM)/(1 - pM)$ , where  $M = (\varepsilon_c - 1)/(\varepsilon_c + 1)$  and  $p = \pi r_c^2/\Lambda_0^2$  is the filling ratio.

For the square array of cylinders, the electrostriction is given by [30]

$$\frac{\partial \varepsilon_{\text{eff}}}{\partial u_{zz}} = -\frac{\varepsilon_{\text{eff}}^2 - 1}{2} \left[ \frac{1 - 1.297pM \cos(2\phi_{\kappa_{\text{eff}}})}{pM} \right], \quad (15)$$

where  $\phi_{\kappa_{\text{eff}}}$  denotes the angle between the wave vector and the  $z$  axis;  $\varepsilon_{\text{eff}} = \sqrt{\varepsilon_{\text{eff},x}^2 + \varepsilon_{\text{eff},z}^2}$  is the “length” of the effective permittivity. The effective permittivity along the  $x$  direction  $\varepsilon_{\text{eff},x}$  and along the  $z$  direction  $\varepsilon_{\text{eff},z}$  are no longer equal due to the deformation (stretch or shear), which breaks the symmetry. Therefore, the electrostrictions are given by

$$\begin{aligned} \frac{\partial \varepsilon_{\text{eff},x}}{\partial u_{zz}} &= \frac{\partial \varepsilon_{\text{eff}}}{\partial u_{zz}} \Big|_{\phi_{\kappa_{\text{eff}}=\frac{\pi}{2}}} = -\frac{(\varepsilon_{\text{eff}} - 1)^2}{2} \frac{1 + 1.297pM}{pM}, \\ \frac{\partial \varepsilon_{\text{eff},z}}{\partial u_{zz}} &= \frac{\partial \varepsilon_{\text{eff}}}{\partial u_{zz}} \Big|_{\phi_{\kappa_{\text{eff}}=0}} = -\frac{(\varepsilon_{\text{eff}} - 1)^2}{2} \frac{1 - 1.297pM}{pM}. \end{aligned} \quad (16)$$

Figure 9 shows the force densities calculated by the MST and HST for two TM polarized incident beams with different incident angles ( $0^\circ$  and  $30^\circ$ ,  $0^\circ$  and  $60^\circ$ ,  $30^\circ$  and  $60^\circ$ , and  $60^\circ$  and  $80^\circ$ ). Clearly, the force densities calculated by HST ( $f_H$  red circles) agree excellently with the benchmarks ( $f_M$  blue stars) computed by MST.

## VI. COMPARISON OF FORCE DENSITIES CALCULATED BY HELMHOLTZ, MINKOWSKI, AND EINSTEIN-LAUB STRESS TENSORS

For comparison, we also consider the Minkowski and Einstein-Laub stress tensors [2–8]. The Minkowski tensor is

$$T_{ik,\text{Min}} = \frac{1}{2} \text{Re} [E_i D_k^* + \mu_0 H_i H_k^* - \frac{1}{2} (\varepsilon_0 \varepsilon_r |\mathbf{E}|^2 + \mu_0 |\mathbf{H}|^2) \delta_{ik}], \quad (17)$$

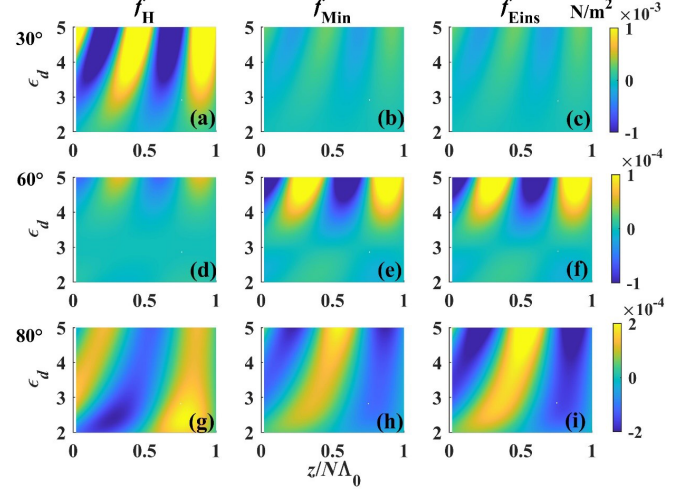


FIG. 10. Contour plot of the optical force densities versus the slab index and permittivity. The incident light is TM polarized. The left, middle, and right columns are  $f_H$ ,  $f_{\text{Min}}$ , and  $f_{\text{Eins}}$ , respectively. The first, second, and third rows denote the results when the incident angles are  $30^\circ$ ,  $60^\circ$ , and  $80^\circ$ .

while the Einstein-Laub stress tensor is

$$T_{ik,\text{Eins}} = \frac{1}{2} \text{Re} [E_i D_k^* + \mu_0 H_i H_k^* - \frac{1}{2} (\varepsilon_0 |\mathbf{E}|^2 + \mu_0 |\mathbf{H}|^2) \delta_{ik}]. \quad (18)$$

In Fig. 10,  $f_H$ ,  $f_{\text{Min}}$ , and  $f_{\text{Eins}}$  denote the internal force densities calculated by Helmholtz, Minkowski, and Einstein-Laub stress tensors, using the scalar effective medium theory for the one-dimensional multilayer structure. The incident light is TM polarized. The left, middle, and right columns denote  $f_H$ ,  $f_{\text{Min}}$ , and  $f_{\text{Eins}}$ , respectively. The first, second, and third rows correspond to the incident angles of  $30^\circ$ ,  $60^\circ$ , and  $80^\circ$ , respectively. It is clear that  $f_{\text{Min}}$  and  $f_{\text{Eins}}$  are not accurate, as they differ from the  $f_H$ . It is in fact not very surprising, as there are no electrostriction and magnetostriction terms in Minkowski and Einstein-Laub stress tensors, leading to the lack of information about the microscopic lattice structure.

## VII. CONCLUSION

For the one-dimensional multilayer structure and 2D square lattice cylinder array, by comparing with the benchmarking MST approach, we showed that the internal optical force densities can be computed accurately by HST, even for multiple incident beams, if the electrostriction and magnetostriction are regarded as operators. Such an approach is expected to work for an arbitrary propagating incident wave, as the wave can be expanded by a series of plane waves. We also demonstrated that Minkowski and Einstein-Laub stress tensors failed in computing the internal optical force densities due to the missing of the information about the lattice structure. This work provides a concise and accurate approach to compute the internal optical force in metamaterials, and helps us to understand the optomechanical effect in metamaterials.

## ACKNOWLEDGMENTS

The authors acknowledge the support of the Open Research Fund of Hunan Provincial Key Laboratory of Flexible Electronic Materials Genome Engineering through Grant No. 202007, the Scientific Research Foundation of Hunan Provincial Education Department through Grant No. 19C0034, the National Natural Science Foundation of China (Grants No. 11304260, No. 12074169, and No. 11904237), and Natural Science Foundation of Guangdong Province (Grant No. 2020A1515010669).

## APPENDIX A: DERIVATION OF EQ. (6)

We shall derive Eq. (6) with the electrostriction and magnetostriction as operators, namely, Eq. (6) in the main text, based on the principles of virtual work.

For a nondispersive medium, such as our effective medium where all the effective constitutive parameters are independent of the frequency, the time-averaged total electromagnetic free energy inside a small square is given by  $W = W_e + W_h = -\frac{1}{4}\text{Re}(\mathbf{E} \cdot \mathbf{D}^* + \mathbf{H} \cdot \mathbf{B}^*)ds$  [31], where  $ds = ab$  is the volume of the area;  $\mathbf{E}$ ,  $\mathbf{D}$ ,  $\mathbf{H}$ , and  $\mathbf{B}$  are the electromagnetic fields inside the area and can be taken as constants since the area is small. Subjecting one of the boundaries (along  $a$ ) of the area to a virtual translation over an infinitesimal distance  $\xi$ , according to the principles of virtual work, the change in the total free energy inside the volume should be equal to the work done by the boundary force  $\sum T_{ik}\xi_i n_k b$ , where  $T_{ik}$  is the surface stress tensor component and  $n_k$  is the unit normal vector component of the boundary. For the magnetic part, one has

$$\sum T_{ik}^h \xi_i n_k b = \delta W_h = \delta W_{h,s} + \delta W_{h,f} + \delta W_{h,p}, \quad (\text{A1})$$

where  $T_{ik}^h$  is the surface stress tensor of the magnetic part;  $\delta W_{h,s}$ ,  $\delta W_{h,f}$ ,  $\delta W_{h,p}$  are variations of the total free energy in-

side  $ds$  due to the changes of the volume, magnetic field, and the effective constitutive parameters, respectively, and they are given by

$$\begin{aligned} \delta W_{h,s} &= -\frac{1}{4}\text{Re}(\mathbf{H} \cdot \mathbf{B}^*)b\mathbf{n} \cdot \boldsymbol{\xi} = -\frac{1}{4}\text{Re}(\mathbf{H} \cdot \mathbf{B}^*)b \sum \delta_{ik}\xi_i n_k, \\ \delta W_{h,f} &= \frac{\partial}{\partial \mathbf{H}} \left[ -\frac{1}{4}\text{Re}(\mathbf{H} \cdot \mathbf{B}^*)ab \right] \delta \mathbf{H} = -\frac{1}{2}\text{Re}(\mathbf{B}^* \cdot \delta \mathbf{H})ab, \\ \delta W_{h,p} &= \sum_m \frac{\partial}{\partial \mu_{\text{eff},m}} \left[ -\frac{1}{4}\text{Re}(\mathbf{H} \cdot \mathbf{B}^*)ab \right] \delta \mu_{\text{eff},m}, \end{aligned} \quad (\text{A2})$$

where  $\delta_{ik}$  is the Kronecker delta function and  $\mu_{\text{eff},m}$  is the effective permeability for the  $m$ th incident plane wave. If the incident beam can be decomposed into infinite plane wave components, we just replace the summation in the third equation of Eq. (A2) by an integration.

Note that the potential of each point on the boundary remains invariant during the deformation [31], namely,  $\mathbf{H}' \cdot \mathbf{n}a + \mathbf{H}' \cdot \boldsymbol{\xi} = \mathbf{H} \cdot \mathbf{n}a$  and  $\mathbf{H}' \times \mathbf{n}b = \mathbf{H} \times \mathbf{n}b$ ; then

$$\begin{aligned} \delta \mathbf{H} &= \mathbf{H}' - \mathbf{H} = (\mathbf{n} \times \delta \mathbf{H}) \times \mathbf{n} + (\delta \mathbf{H} \cdot \mathbf{n})\mathbf{n} \\ &= -(\mathbf{H}' \cdot \boldsymbol{\xi})\mathbf{n}/a = -(\mathbf{H} \cdot \boldsymbol{\xi})\mathbf{n}/a. \end{aligned} \quad (\text{A3})$$

Here we used  $(\mathbf{n} \times \delta \mathbf{H}) \times \mathbf{n} = (\mathbf{n} \cdot \mathbf{n})\delta \mathbf{H} - (\delta \mathbf{H} \cdot \mathbf{n})\mathbf{n}$ . Substituting Eq. (A3) into the second equation of Eq. (A2), we obtain

$$\delta W_{h,f} = \frac{1}{2}\text{Re}(\mathbf{n} \cdot \mathbf{B}^*)(\mathbf{H} \cdot \boldsymbol{\xi})b = \frac{1}{2} \sum \text{Re}(H_i B_k^*) \xi_i n_k. \quad (\text{A4})$$

For the third equation of Eq. (A2), one applies

$$\mathbf{H} = \sum_n \mathbf{H}_n, \quad \mathbf{B} = \sum_n \mu_{\text{eff},n} \mathbf{H}_n, \quad (\text{A5})$$

where  $\mathbf{H}_n$  is the magnetic field due to the  $n$ th incident plane wave. A simple proof of Eq. (A5) is given in Appendix B. One arrives at

$$\begin{aligned} \delta W_{h,p} &= -\frac{1}{4}\text{Re} \left[ \left( \sum_n \mathbf{H}_n \right) \cdot \sum_m \frac{\partial}{\partial \mu_{\text{eff},m}} \left( \sum_n \mu_{\text{eff},n} \mathbf{H}_n ab \right) \delta \mu_{\text{eff},m} \right], \\ &= -\frac{1}{4}\text{Re} \left[ \left( \sum_n \mathbf{H}_n \right) \cdot \left( \sum_m \mathbf{H}_m \delta \mu_{\text{eff},m} \right) ab \right]. \end{aligned} \quad (\text{A6})$$

Note that

$$\delta \mu_{\text{eff},m} = \frac{\partial \mu_{\text{eff},m}}{\partial u_{ik}} u_{ik}, \quad (\text{A7})$$

where

$$u_{ik} = \frac{1}{2} \left( \frac{\partial u_i}{\partial x_k} + \frac{\partial u_k}{\partial x_i} \right) = \frac{1}{2a} (\xi_i n_k + \xi_k n_i) = \frac{1}{a} \xi_i n_k \quad (\text{A8})$$

is the strain tensor which is symmetric. Then Eq. (A6) can be rewritten as

$$\delta W_{h,p} = -\frac{1}{4}\text{Re} \left( \sum_n \mathbf{H}_n \right) \cdot \left( \sum_m \frac{\partial \mu_{\text{eff},m}}{\partial u_{ik}} \mathbf{H}_m \right) \xi_i n_k b. \quad (\text{A9})$$

Combining Eqs. (A2), (A4), and (A9), we arrive at

$$T_{ik,H} = \frac{1}{2}\text{Re} \left\{ H_i B_k^* - \frac{1}{2}(\mathbf{H} \cdot \mathbf{B}^*)\delta_{ik} - \frac{1}{2}\mathbf{H} \cdot \sum_n \frac{\partial \mu_{\text{eff},n}}{\partial u_{ik}} \mathbf{H}_n \right\}. \quad (\text{A10})$$

The electric counterpart of the stress tensor can be obtained similarly and then we can obtain the full expression of the stress tensor as Eq. (6) in the main text.

## APPENDIX B: PROOF OF EQ. (A5)

For a nonlocal medium where the constitutive parameters are  $k$  dependent, the magnetic induction field is

expressed as

$$\mathbf{B} = \int \tilde{\mu}_{\text{eff}}(\mathbf{x} - \mathbf{x}') \mathbf{H}(\mathbf{x}') d^3 \mathbf{x}' = F^{-1}[\mu_{\text{eff}}(k') \tilde{\mathbf{H}}(k')], \quad (\text{B1})$$

where the convolution theorem has been applied,  $F^{-1}$  denotes the inverse Fourier transform,  $\tilde{\mu}_{\text{eff}}$  is the inverse Fourier transform of  $\mu_{\text{eff}}$ , and  $\tilde{\mathbf{H}}$  is the Fourier transform of  $\mathbf{H}$ . Suppose the magnetic field is decomposed into multiple plane waves:

$$\mathbf{H}(\mathbf{x}) = \sum_n \mathbf{H}_n(\mathbf{x}) = \sum_n a_n e^{i\mathbf{k}_n \cdot \mathbf{x}}. \quad (\text{B2})$$

Its Fourier transform  $\tilde{\mathbf{H}}$  is

$$\begin{aligned} \tilde{\mathbf{H}} &= \frac{1}{(2\pi)^{3/2}} \int \sum_n a_n e^{i\mathbf{k}_n \cdot \mathbf{x}} e^{-i\mathbf{k} \cdot \mathbf{x}} d\mathbf{x}^3 \\ &= (2\pi)^{3/2} \sum_n a_n \delta(\mathbf{k} - \mathbf{k}_n). \end{aligned} \quad (\text{B3})$$

Substituting Eq. (B3) into Eq. (B1), we obtain

$$\begin{aligned} \mathbf{B} &= \sum_n \int \mu_{\text{eff}}(\mathbf{k}) a_n \delta(\mathbf{k} - \mathbf{k}_n) e^{i\mathbf{k} \cdot \mathbf{x}} d\mathbf{k}^3 = \sum_n \mu_{\text{eff}}(\mathbf{k}_n) a_n e^{i\mathbf{k}_n \cdot \mathbf{x}} \\ &= \sum_n \mu_{\text{eff}}(\mathbf{k}_n) \mathbf{H}_n(\mathbf{x}) = \sum_n \mu_{\text{eff},n} \mathbf{H}_n(\mathbf{x}), \end{aligned} \quad (\text{B4})$$

where  $\mu_{\text{eff},n} = \mu_{\text{eff}}(\mathbf{k}_n)$ .

- 
- [1] J. A. Stratton, *Electromagnetic Theory* (McGraw-Hill, New York, 1941).
- [2] H. Minkowski, *Nachr. Ges. Wiss. Goettingen, Math. Phys. K* **1**, 53 (1908).
- [3] H. Minkowski, *Math. Ann.* **68**, 472 (1910).
- [4] M. Abraham, *Rend. Circ. Mat. Palermo* **28**, 1 (1909).
- [5] M. Abraham, *Rend. Circ. Mat. Palermo* **30**, 33 (1910).
- [6] A. Einstein and J. Laub, *Ann. Phys.* **331**, 541 (1908).
- [7] H. Helmholtz, *Ann. Phys.* **249**, 385 (1881).
- [8] L. D. Landau, E. M. Lifshitz, and L. P. Pitaevskii, *Electrodynamics of Continuous Media*, 2nd ed. (Butterworth-Heinemann, New York, 1984).
- [9] U. Leonhardt, *Nature (London, UK)* **444**, 823 (2006).
- [10] R. N. C. Pfeifer, T. A. Nieminen, N. R. Heckenberg, and H. Rubinsztein-Dunlop, *Rev. Mod. Phys.* **79**, 1197 (2007).
- [11] I. Liberal, I. Ederra, R. Gonzalo, and R. W. Ziolkowski, *Phys. Rev. A* **88**, 053808 (2013).
- [12] M. Mansuripur, A. R. Zakharian, and E. M. Wright, *Phys. Rev. A* **88**, 023826 (2013).
- [13] V. Kajorndejnukul, W. Ding, S. Sukhov, C. W. Qiu, and A. Dogariu, *Nat. Photonics* **7**, 787 (2013).
- [14] A. M. Jazayeri and K. Mehrany, *Phys. Rev. A* **89**, 043845 (2014).
- [15] C. W. Qiu, W. Ding, M. R. C. Mahdy, D. Gao, T. Zhang, F. C. Cheong, A. Dogariu, Z. Wang, and C. T. Lim, *Light Sci. Appl.* **4**, e278 (2015).
- [16] N. G. C. Astrath, L. C. Malacarne, M. L. Baesso, G. V. B. Lukasiewicz, and S. E. Bialkowski, *Nat. Commun.* **5**, 4363 (2014).
- [17] K. Ding and C. T. Chan, *Phys. Rev. B* **97**, 155118 (2018).
- [18] S. M. Barnett, *Phys. Rev. Lett.* **104**, 070401 (2010).
- [19] A. V. Poshakinskiy and A. N. Poddubny, *Phys. Rev. X* **9**, 011008 (2019).
- [20] J. Zhang, K. MacDonald, and N. Zheludev, *Light Sci. Appl.* **2**, e96 (2013).
- [21] B. F. Kennedy, P. Wijesinghe, and D. D. Sampson, *Nat. Photonics* **11**, 215 (2017).
- [22] T. Zhao, Ph.D. thesis and dissertation, The University of Iowa, Graduate College, 2015.
- [23] V. M. Agranovlch and V. E. Kravtsov, *Solid State Commun.* **55**, 85 (1985).
- [24] P. A. Belov, *Microwave Opt. Technol. Lett.* **37**, 259 (2003).
- [25] D. R. Smith and D. Schurig, *Phys. Rev. Lett.* **90**, 077405 (2003).
- [26] I. V. Lindell, S. A. Tretyakov, K. I. Nikoskinen, and S. B. W. Ilvonen, *Microwave Opt. Technol. Lett.* **31**, 129 (2001).
- [27] A. Poddubny, I. Iorsh, P. Belov, and Y. Kivshar, *Nat. Photonics* **7**, 948 (2013).
- [28] N. Wang, S. B. Wang, Z. Q. Zhang, and C. T. Chan, *Phys. Rev. B* **98**, 045426 (2018).
- [29] N. Wang, S. B. Wang, and J. Ng, *Phys. Rev. A* **97**, 033839 (2018).
- [30] W. J. Sun, S. B. Wang, J. Ng, L. Zhou, and C. T. Chan, *Phys. Rev. B* **91**, 235439 (2015).
- [31] L. D. Landau, E. M. Lifshitz, and L. P. Pitaevskii, *Electrodynamics of Continuous Media*, 2nd ed. (Butterworth-Heinemann, New York, 1984).
- [32] I. Brevik, *Phys. Rep.* **52**, 133 (1979).
- [33] P. Penfield and H. A. Haus, *Electrodynamics of Moving Media* (The MIT Press, Cambridge, 1967).
- [34] R. A. Anderson, *Phys. Rev. B* **33**, 1302 (1986).
- [35] Y. M. Shkel and D. J. Klingenberg, *J. Appl. Phys.* **80**, 4566 (1996).
- [36] Y. M. Shkel and D. J. Klingenberg, *J. Appl. Phys.* **83**, 7834 (1998).
- [37] H. Y. Lee, Y. Y. Peng, and Y. M. Shkel, *J. Appl. Phys.* **98**, 074104 (2005).
- [38] Y. M. Shkel, *Philos. Mag.* **87**, 1743 (2007).
- [39] L. D. Landau and E. M. Lifshitz, *Theory of Elasticity*, 3rd ed. (Butterworth-Heinemann, New York, 1999).